Calibrated Residual Intelligence for Intra-Procedural CBCT–Based Collateral Grading in Ischemic Stroke

Kazi Ashikur Rahman[1], Nur Hasanah Ali[2]*,
Ahmad Sobri Muda[3], Nur Asyiqin Amir Hamzah[4], Noradzilah Ismail[5]
Faculty of Electrical Engineering Technology,
Universiti Teknikal Malaysia Melaka (UTeM), Melaka, Malaysia[1]
Faculty of Engineering and Technology (FET), Multimedia University, Melaka, Malaysia[2,4]
Faculty of Medicine and Health Sciences, Department of Imaging, Universiti Putra Malaysia, Selangor, Malaysia[3]
Faculty of Information Science and Technology (FIST), Multimedia University, Melaka, Malaysia[5]

***Abstract*—Brain stroke occurs when the brain's blood supply is disrupted, leading to oxygen deprivation and rapid neuronal death. Ischemic stroke, the focus of this study, accounts for most cases and is strongly influenced by collateral circulation, a network of alternative vessels that stabilize perfusion when a primary artery is obstructed. Collateral status determines the extent of salvageable tissue and is typically graded manually using modalities such as magnetic resonance angiography (MRA), computed tomography (CT), and cone-beam computed tomography (CBCT), a process prone to subjectivity and inter-observer variability. This study proposes a ResNet-18–based deep learning framework for automated three-class classification of collateral circulation (Good, Moderate, Poor) from intra-procedural CBCT scans. A curated dataset of 45 patient cases (22,861 DICOM slices), annotated by an expert neuroradiologist, was preprocessed with patient-wise partitioning, normalization, and augmentation. The model achieved a validation accuracy of 88.8%, a micro-averaged precision–recall score of 0.947, and a macro-averaged ROC AUC of 0.958. Calibration analysis confirmed well-aligned probability estimates, while most misclassifications occurred in the Moderate class, reflecting inherent clinical ambiguity. Compared with prior CBCT studies using shallower architectures, the proposed framework demonstrates substantially higher accuracy, improved calibration, and enhanced robustness. These findings highlight the feasibility of ResNet-18 applied to CBCT imaging as a reliable and efficient tool to support neuroradiologists in collateral grading during hyperacute stroke management**

***Keywords*—Collateral circulation; brain stroke; ischemic stroke; deep learning; ResNet-18**

I. Introduction

Ischemic stroke occurs when a cerebral blood vessel becomes obstructed, typically by a thrombus, thereby interrupting the supply of oxygen and nutrients. Without prompt intervention, this blockage can cause irreversible neuronal damage within minutes, leading to severe neurological deficits [1], [2]. Globally, Ischemic stroke is a major public health challenge, accounting for over 80% of stroke cases worldwide and affecting more than 12 million people annually [3][4][5]. It remains a leading cause of death, long-term disability, and healthcare burden. These realities underscore the urgent need for improved methods of early diagnosis, prognosis, and treatment to mitigate long-term disability and improve patient outcomes.

*Corresponding author.

Collateral circulation serves as the brain's primary compensatory mechanism during arterial occlusion. Networks such as the Circle of Willis and leptomeningeal anastomoses sustain perfusion and preserve the penumbra during arterial occlusion [6], [7], [8]. In addition to arterial routes, venous and lymphatic systems are increasingly recognized as contributors to intracranial homeostasis under ischemic stress [9]. Patients with robust collaterals typically demonstrate slower infarct progression and extended therapeutic windows for both intravenous thrombolysis and mechanical thrombectomy [10], [11], [12]. Consequently, collateral status has emerged as a critical prognostic marker and a key determinant in acute stroke treatment decisions.

Neuroimaging plays a central role in collateral evaluation. Conventional methods rely on computed tomography angiography (CTA) and magnetic resonance angiography (MRA), with cone-beam computed tomography (CBCT) emerging as a promising intra-procedural alternative. However, manual collateral grading is time-consuming, subjective, and limited by inter-observer variability. To overcome these challenges, deep learning offers the potential for automated, consistent, and scalable assessment. Convolutional neural networks (CNNs), including architectures such as ResNet-18, have demonstrated strong performance in diverse medical imaging tasks ranging from pneumonia detection [13] to retinal-based kidney disease screening [14]. More recently, CNN-based approaches have been applied to collateral circulation grading in CTA, MRA, and CBCT, laying the groundwork for robust, clinically integrated decision-support systems. Building on this foundation, this study investigates ResNet-18 for automated tri-class classification of collateral circulation (Good, Moderate, Poor) in ischemic stroke patients using intra-procedural CBCT. The following sections provide the clinical background, describe the methodological design, and evaluate the performance of the proposed framework in comparison with existing approaches. This study addresses the challenge of subjective and time-consuming collateral grading by proposing an automated CBCT-based deep learning approach for three-class collateral classification. The main difficulty lies in CBCT intensity variations and the visual overlap between Moderate and adjacent grades, which can reduce precision.

The remainder of this study is organized as follows: Section II reviews stroke and collateral background and imaging modalities; Section III summarizes related work; Section IV nd

Section V describes the methodology and dataset; Section VI presents experimental results; Section VII discusses findings and limitations; and Section VIII concludes the study.

II. Brain Stroke

Stroke occurs when the blood supply to a part of the brain is disrupted, leading to oxygen deprivation and rapid death of brain cells [15]. The brain is essential for coordinating movements, preserving memories, generating thoughts and emotions, and enabling speech and language functions [16]. It also regulates critical bodily processes such as breathing and digestion. To perform these functions effectively, the brain depends on a continuous flow of oxygen-rich blood delivered through its intricate arterial system. When this flow is blocked or reduced, brain tissue rapidly sustains damage [17]. Without timely restoration of blood supply, affected regions may suffer permanent injury or death, resulting in lasting disability or fatality. Strokes are broadly classified into two major types based on their underlying mechanisms: hemorrhagic stroke and ischemic stroke. Fig. 1 illustrates the fundamental differences between these two types.

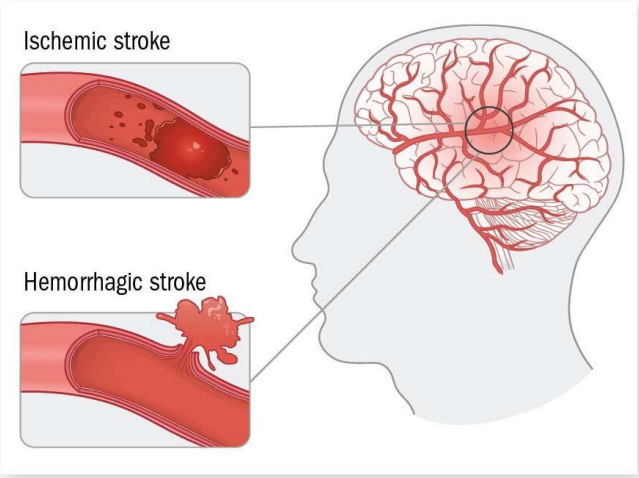

Fig. 1. Comparison between ischemic stroke (arterial blockage) and hemorrhagic stroke (vessel rupture) [18].

A. Hemorrhagic Stroke

Hemorrhagic stroke occurs when a weakened blood vessel ruptures, causing bleeding into the brain tissue [19]. The accumulation of blood elevates intracranial pressure, compresses brain structures, and diminishes downstream blood flow. Although hemorrhagic strokes are less common than ischemic strokes, they are associated with higher early mortality rates. Management of hemorrhagic stroke focuses on controlling bleeding, alleviating intracranial pressure, and preventing complications such as rebleeding and hydrocephalus. Since hemorrhagic stroke arises from vessel rupture rather than occlusion, collateral circulation does not play a central role in its clinical management [20]. Accordingly, research into collateral blood flow restoration is less applicable to hemorrhagic stroke. For this reason, the present work primarily emphasizes ischemic stroke, where collateral circulation is critically important for sustaining tissue survival and improving recovery outcomes.

B. Ischemic Stroke

Ischemic stroke, accounting for approximately 85% of all stroke cases, results from obstruction of a cerebral artery, most commonly due to thrombosis or embolism [21]. The sudden interruption of blood flow initiates a cascade of cellular injury and metabolic dysfunction, ultimately leading to infarction if untreated. Collateral circulation, the network of auxiliary vessels capable of supplying blood to ischemic brain regions, emerges as a crucial determinant of stroke severity and recovery potential [22]. Well-developed collateral networks can sustain perfusion to the ischemic penumbra, delay infarct progression, and extend the therapeutic window for interventions. Consequently, evaluation and optimization of collateral pathways have become central themes in ischemic stroke research. In this context, the present study focuses on ischemic stroke, aiming to advance automated methods for collateral circulation assessment and improve decision-making in hyperacute stroke management.

C. Collateral Circulation in Ischemic Stroke

Collateral circulation refers to a network of alternative blood vessels that can provide compensatory blood flow when a primary cerebral artery is obstructed. This auxiliary pathway helps stabilize cerebral perfusion and can determine the extent of salvageable tissue, or the ischemic penumbra, during a stroke [6], [23]. Fig. 2 illustrates how collateral vessels bypass a thrombus obstructing a major artery, thereby sustaining blood supply to downstream regions.

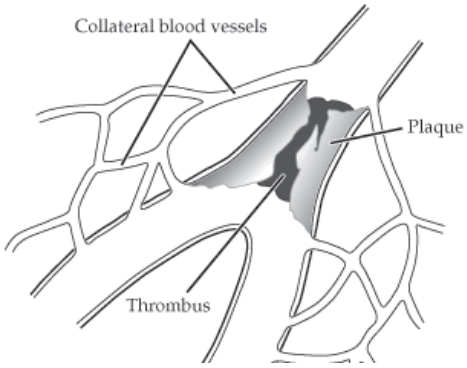

Fig. 2. Schematic showing collateral blood vessels bypassing a thrombus obstructing a primary cerebral artery [24].

The adequacy of collateral circulation varies considerably between individuals and is influenced by vascular anatomy, age, and comorbidities. Patients with good collateral status often demonstrate smaller infarct cores and better clinical outcomes, while poor collaterals are linked to rapid infarct progression and worse prognosis [8], [25]. Fig. 4 and Fig. 3 shows that Good collaterals allow sufficient blood rerouting to preserve tissue, whereas poor collaterals fail to maintain adequate perfusion, leading to irreversible injury.

Currently, collateral grading is performed manually by radiologists who visually interpret magnetic resonance angiography (MRA), computed tomography (CT), cone-beam computed tomography (CBCT), or digital subtraction angiography (DSA) scans. However, this process is inherently subjective, time-consuming, and prone to inter-observer variability. Given

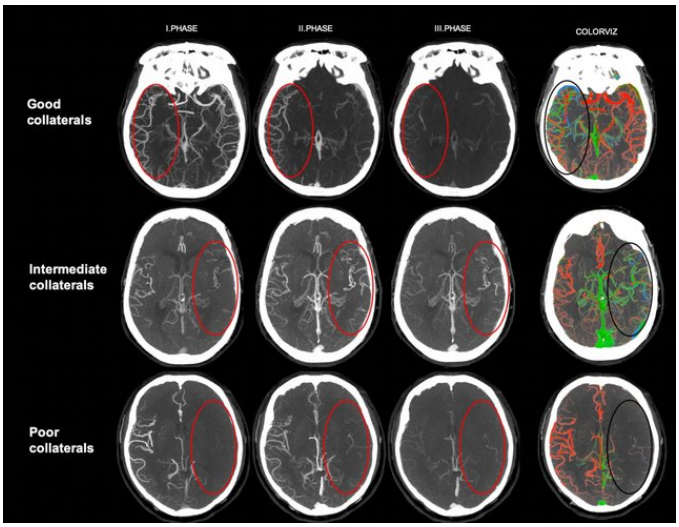

Fig. 3. Multiphase assessment of collateral circulation: Good (top), intermediate (middle), and poor (bottom), with corresponding color-coded visualization [26].

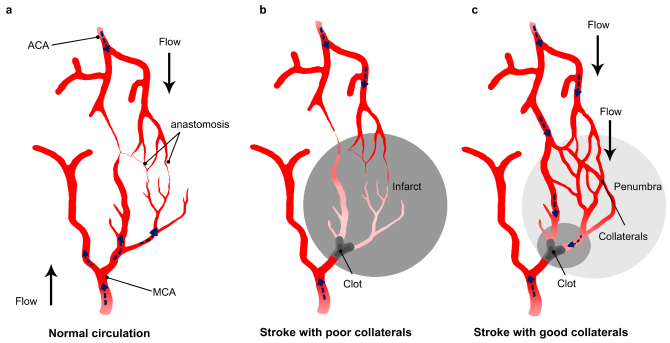

Fig. 4. Classification of collateral circulation: a) Normal circulation, b) Stroke with poor collaterals, c) Stroke with good collaterals [27]. (Image adapted under a CC BY 4.0 license).

the prognostic importance of collateral status, there is a clear need for automated and reliable classification methods. To address this gap, the present study introduces a ResNet-18 deep learning framework designed to classify collateral circulation into Good, Moderate, or Poor, thereby reducing variability and supporting clinicians in urgent decision-making.

D. Imaging Modalities for Collateral Assessment

Several imaging modalities are currently used to evaluate collateral circulation, including computed tomography angiography (CTA), magnetic resonance angiography (MRA), cone-beam computed tomography (CBCT), and digital subtraction angiography (DSA). CTA is fast and widely available, with multiphase protocols capable of capturing delayed collateral filling [28]. MRA provides radiation-free vascular imaging but is slower and less practical in acute settings [29]. DSA remains the invasive reference standard for visualizing cerebral vasculature. CBCT has recently emerged as a promising intra-procedural tool, offering high-resolution three-dimensional visualization directly in the angiography suite and the potential to complement standard CT and MRI during endovascular workflows [30], [31].This comparison highlights CBCT's suitability for intra-procedural stroke workflows, where rapid acquisition and integration with endovascular treatment are critical, unlike CT and MRI which are typically pre-procedural.

Table I provides a general comparison of CBCT, CT, and MRI. Although most reported advantages of CBCT, such as lower radiation exposure, shorter scan time, and reduced cost, have been derived from dental and general radiology literature, these features suggest potential benefits for neurointerventional use as well. However, stroke- and neurointervention-specific head-to-head studies remain limited, and thus these characteristics should be interpreted cautiously when extrapolated to acute cerebrovascular workflows.

Recent CBCT-based studies have applied deep learning models for collateral classification. For example, Ali et al. [38] employed a ResNet-18 architecture and reported moderate performance, while a subsequent study using VGG11 [39] also achieved only modest accuracy. These results highlight both the feasibility of CBCT for automated collateral grading and the clear need for methodological improvements. In this study, we aim to enhance classification performance by leveraging a deeper residual network (ResNet-18), incorporating a larger dataset, and applying advanced augmentation techniques to improve generalization.

The next section reviews prior research on collateral circulation classification across different modalities to contextualize the present work.

III. Related Work

Most existing studies on collateral circulation assessment in ischemic stroke have focused on deep learning applied to computed tomography (CT) and magnetic resonance imaging (MRI). These modalities are widely used due to their high-quality depiction of brain structures and vascular networks [34], [37]. More recently, cone-beam computed tomography (CBCT) has been explored, but the reported results remain modest compared to CTA and MRI.

For example, Ali et al. [39] applied VGG11 to CBCT images of ischemic stroke patients, using a dataset of 4,368 slices (80% training, 20% testing) for binary classification of good versus poor collaterals. The model achieved only 58.3% accuracy, with sensitivity of 75.5%, specificity of 44.1%, and F1-score of 62.1%. Similarly, Ali et al. [38] employed a pre-trained ResNet-18 on 30 patients (4,368 CBCT slices), reporting 65.9% accuracy, with sensitivity of 0.776, specificity of 0.526, and F1-score of 0.698. Both studies demonstrated feasibility, but were hindered by small datasets, minimal augmentation, and overfitting, which limited generalizability.

Other researchers have explored multimodal and advanced architectures. Tetteh et al. [43] used MR perfusion images from 183 patients, applying reinforcement learning for ROI detection and CNN/ML classifiers, achieving 72% accuracy, but facing challenges of class imbalance and ROI precision. Raj et al. [41] proposed a multimodal CTA-based framework combining ResNet-50 with AutoML, reaching 94.12% accuracy but relying on single-center data. Tan et al. [42] developed a feature-fusion attention network for multiphase CTA, achieving 90.43% accuracy. While these approaches

TABLE I. COMPARISON OF CBCT, CT, AND MRI CHARACTERISTICS IS MAINLY BASED ON DENTAL AND GENERAL RADIOLOGY REPORTS. SINCE STROKE-SPECIFIC EVIDENCE IS LIMITED, THESE VALUES SHOULD BE INTERPRETED CAUTIOUSLY FOR ACUTE CEREBROVASCULAR WORKFLOWS.

Criteria	CBCT	CT	MRI
Working Principle	Uses X-ray computed tomography with divergent beam and 360° rotation [32]	Uses multiple X-rays from different angles [33]	Uses magnetic fields and RF pulses [34]
Resolution	High spatial resolution [32]	Better contrast resolution [32]	Good contrast resolution [34]
Scanning Time	Lower scanning time [35]	Moderate scanning time [35]	Longest scanning time [35]
Cost	Lower cost [36]	Moderate cost [36]	Highest cost [36]
X-ray Beam Coverage	Beam can be collimated to the area of interest [37]	Full area scan [37]	Full area scan [36]
Display Mode	High anatomical precision and diagnostic function [37]	Lower anatomical detail [37]	High-quality images for soft tissue and ligaments [34]

TABLE II. SUMMARY OF COLLATERAL CIRCULATION CLASSIFICATION STUDIES USING AI TECHNIQUES

Study	Modality	Purpose	Method	Key Result
[40]	4D-CTA	Classification	ResNet34 (single vs. multi-image)	AUC 0.85–0.89
[41]	CTA	Classification	Multimodal DL + AutoML	Acc 91.2–94.1%
[42]	CTA (multiphase)	Classification	Fusion attention (CCA4CTA)	Acc 90.4%
[43]	MRI	Classification	CNN + ML (RF, SVM, k-NN)	Acc 72% (CNN)
[44]	CTA	Classification	CNN-SVM, ResNet, ViTs	Acc 62–77%
[39]	CBCT	Classification	VGG11	Acc 58.3%
[38]	CBCT	Classification	ResNet18	Acc 65.9%

demonstrate the potential of advanced architectures, they are primarily based on CTA/MRA datasets rather than CBCT.

Table II summarizes representative approaches, imaging modalities, and reported outcomes. Collectively, these studies show that while CTA and MRI dominate current research, CBCT is emerging as a clinically advantageous modality due to its real-time intra-procedural capability, reduced radiation, lower cost, and availability in the angiography suite. However, CBCT-based deep learning models remain underexplored and have so far achieved only moderate accuracy.

To address this gap, the present study leverages CBCT imaging combined with a residual architecture, ResNet-18. By using a larger dataset, applying systematic data augmentation, and moving beyond binary classification to a clinically relevant three-class grading (*Good*, *Moderate*, *Poor*), this work aims to significantly improve accuracy, calibration, and generalizability. The following section details the methodology of the proposed framework.

IV. METHODS

The overall methodology of the proposed study is summarized in Fig. 5. The pipeline begins with dataset collection from Hospital Sultan Abdul Aziz Shah, Universiti Putra Malaysia (UPM), followed by preprocessing steps such as bone removal, normalization, and noise reduction. Data augmentation was then applied to increase variability, and the dataset was partitioned into training and validation subsets. The ResNet-18 model, initialized with ImageNet weights, was trained and fine-tuned for three-class collateral classification. A patient-wise split ensured that slices from the same patient did not appear in both training and validation sets, preventing data leakage. The implementation was carried out in Python with TensorFlow/Keras on an RTX 3090 GPU. The study followed a supervised learning design with neuroradiologist-annotated labels, patient-wise partitioning to prevent leakage, and a two-phase fine-tuning strategy to balance generalization and class separability.

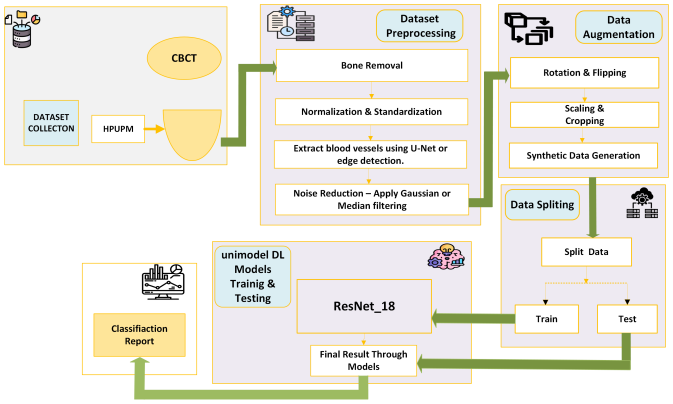

Fig. 5. Overall methodology for CBCT-based collateral circulation classification using ResNet-18.

Experiments were conducted using Python 3.10 with TensorFlow 2.12/Keras, NumPy 1.26, and scikit-learn 1.4 on an RTX 3090 (24 GB) with CUDA 11.8/cuDNN 8.9. Model performance was assessed using accuracy, precision, recall (sensitivity), specificity, F1-score, PR-AUC, ROC-AUC, and calibration analysis.

V. DATASET

For this study, the dataset was obtained from Hospital Sultan Abdul Aziz Shah, Universiti Putra Malaysia (UPM).

It consists of cone-beam computed tomography (CBCT) scans acquired from patients diagnosed with ischemic stroke. A total of 45 cases were included, each containing a full volumetric series of axial slices. Each patient was assigned a unique identifier and accession number, and all metadata were securely documented to maintain proper traceability. Annotation of the dataset was carried out by an experienced neuroradiologist (Dr. Ahmad Sobri Muda), who categorized each patient into one of three clinically meaningful grades of collateral circulation: Good, Moderate, and Poor. The final distribution comprised 13 patients in the Good category, 13 in the Moderate category, and 19 in the Poor category.

The demographic composition of the cohort is summarized in Table III. Overall, the dataset included 18 females and 27 males, with gender distribution remaining relatively balanced across the three collateral circulation groups. In total, the dataset comprised 22,861 DICOM slices, with each patient contributing approximately 350–400 slices. This volume is consistent with the coverage typically required in neurovascular CBCT examinations. For model development, the dataset was partitioned on a patient-wise basis into 70% for training and 30% for testing, ensuring that slices from the same subject did not appear in both sets. The dataset used in this study is available from the corresponding author upon reasonable request.

TABLE III. PATIENT DISTRIBUTION BY COLLATERAL CLASS AND GENDER

Class	Female	Male	Total
Good	5	8	13
Moderate	6	7	13
Poor	7	12	19
Total	**18**	**27**	**45**

Although the macro-averaged precision was 0.8634, this value should be interpreted in the context of clinical ambiguity, particularly within the Moderate collateral class. Precision was reduced primarily due to overlap between Moderate and adjacent classes, a challenge also reported in neuroradiologist-based grading. Several design choices were introduced to improve precision: patient-wise data partitioning eliminated slice-level leakage, class weighting mitigated imbalance, label smoothing reduced over-confident predictions, and realistic data augmentation improved generalization. These strategies enhanced precision while maintaining balanced recall and well-calibrated probabilities.

A. Preprocessing

The preprocessing stage aimed to prepare raw cone-beam computed tomography (CBCT) data for deep learning analysis. First, all volumes in DICOM format were checked to remove incomplete or corrupted slices [45]. The remaining valid scans were annotated by a neuroradiologist into three categories: *Good*, *Moderate*, and *Poor* collateral status.

To enable compatibility with deep learning frameworks, DICOM files were converted into lossless `.png` format using a custom Python script. This conversion preserved grayscale vascular details and allowed faster I/O operations. The converted images were stored in class-specific directories for traceability during training and evaluation.

Each slice was resized to 224×224 pixels and normalized to the $[0, 1]$ range using min–max scaling:

$$I_{\text{norm}}(x, y) = \frac{I(x, y) - I_{\text{min}}}{I_{\text{max}} - I_{\text{min}}},$$

where, $I(x, y)$ denotes the pixel intensity and I_{min}, I_{max} are dataset-level minimum and maximum values.

A patient-wise split strategy was applied so that slices from the same subject appeared in only one subset (training, validation, or testing), preventing data leakage and ensuring reliable model evaluation. Additional transformations for data augmentation were later applied to increase dataset variability and improve model generalization, as described in the next subsection.

B. Data Augmentation

To increase dataset diversity and mitigate overfitting, stochastic augmentation functions were applied to the CBCT slices during training. These transformations were formulated to introduce controlled variability in spatial and photometric domains while preserving the vascular structures essential for clinical interpretation.

Let $I(x, y)$ denote the original image intensity at spatial coordinates (x, y). A horizontal reflection was applied with probability $p = 0.5$, expressed as:

$$I'(x, y) = I(W - x, y), \quad x \in [0, W],\ y \in [0, H],$$

where, W and H represent the image width and height, respectively. This transformation enforces invariance to left–right orientation without altering anatomical fidelity.

Photometric perturbations were introduced through random brightness and contrast adjustments. Brightness variation was modeled as an additive shift:

$$I'(x, y) = I(x, y) + \Delta_b,$$

with $\Delta_b \sim \mathcal{U}(-\beta, \beta)$, $\beta = 0.10$ representing a 10% dynamic range adjustment. Contrast scaling was applied multiplicatively:

$$I'(x, y) = \alpha \cdot I(x, y),$$

where, $\alpha \sim \mathcal{U}(0.9, 1.1)$ governs the rescaling of intensity distributions. Combined, these yield the affine photometric transformation:

$$I'(x, y) = \alpha \cdot I(x, y) + \Delta_b,$$

which models scanner-dependent variations in illumination and detector sensitivity.

A geometric zoom operation was further incorporated by random cropping followed by resizing to the original resolution. For a scaling factor $z \sim \mathcal{U}(0.9, 1.0)$, the effective mapping can be written as:

$$I'(x, y) = I\left(\left\lfloor \frac{x}{z} \right\rfloor, \left\lfloor \frac{y}{z} \right\rfloor\right),$$

where, coordinates outside the valid domain are handled through zero-padding. This introduces local spatial distortions equivalent to minor variations in field of view or patient positioning during acquisition.

Collectively, these augmentations form a nonlinear transformation set $\mathcal{T} = \{T_{\text{flip}}, T_{\text{bright}}, T_{\text{contrast}}, T_{\text{zoom}}\}$, where each image I is stochastically mapped to an augmented sample $I' = T(I)$ with $T \sim \mathcal{U}(\mathcal{T})$. By enforcing the model to learn under this expanded input distribution, the convolutional network is guided to extract invariant vascular patterns rather than memorizing subject-specific intensity or positional artifacts, thereby strengthening generalization.

C. Classification Model: ResNet-18

ResNet-18 was employed as the backbone network to classify collateral circulation from CBCT images into three categories: *Good*, *Moderate*, and *Poor*. Compared with deeper variants such as ResNet-50, ResNet-18 is shallower with 18 layers but preserves the residual learning mechanism that addresses vanishing gradients and supports stable training. Its balance of computational efficiency and representational power makes it well suited for datasets of moderate size. The overall workflow is shown in Fig. 6. ResNet-18 was selected to match the study's data regime: with 45 patient cases, it provides an effective balance of computational efficiency and discriminative power. The residual design supports stable optimization, and the shallower depth reduces overfitting risk relative to deeper backbones.

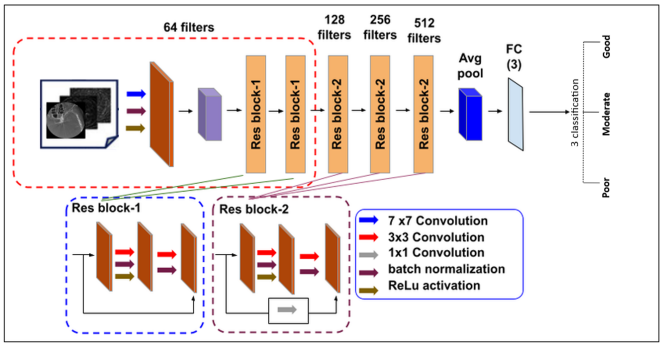

Fig. 6. ResNet-18 framework for CBCT-based collateral circulation classification, consisting of convolutional layers, residual blocks, pooling operations, and a softmax classifier.

1) Model architecture: The model processes preprocessed and augmented CBCT slices, each resized to 224×224 pixels with three channels. The initial stem of the network applies a 7×7 convolution with stride 2, followed by batch normalization, ReLU activation, and 3×3 max-pooling. For an input $X \in \mathbb{R}^{224\times224\times3}$, the first feature representation is computed as Eq. (1):

$$F^{(1)} = \sigma\big(\mathrm{BN}(W^{(1)} * X + b^{(1)})\big), \tag{1}$$

where, $*$ denotes convolution, $W^{(1)}$ and $b^{(1)}$ are the kernel and bias of the first layer, $\mathrm{BN}(\cdot)$ represents batch normalization, and $\sigma(z) = \max(0, z)$ is the ReLU activation.

The core of ResNet-18 is built from basic residual blocks, each consisting of two 3×3 convolutional layers with batch normalization and ReLU, plus an identity shortcut. A residual block computes [see Eq. (2)]:

$$H(x) = \sigma\Big(\mathrm{BN}(W_2 * \sigma(\mathrm{BN}(W_1 * x))) + x\Big), \tag{2}$$

where, W_1 and W_2 are convolution kernels of size 3×3. If the input and output dimensions differ, a 1×1 convolution is applied on the shortcut path. These residual connections enforce stable gradient propagation and allow the block to approximate $H(x) \approx F(x) + x$.

Spatial dimensionality reduction is performed by max pooling [see Eq. (3)]:

$$F_l^{pool} = \max_{(i,j)\in R} F_{i,j}^{(l)}, \tag{3}$$

where, R is the pooling window region. This preserves dominant activations while reducing computational complexity.

After the residual stages, global average pooling (GAP) compresses each feature map into a scalar [see Eq. (4)]:

$$g_k = \frac{1}{H \times W} \sum_{i=1}^{H} \sum_{j=1}^{W} F_{i,j,k}^{(L)}, \tag{4}$$

where, $F_{i,j,k}^{(L)}$ is the activation at spatial location (i, j) in channel k. The resulting feature vector $\mathbf{g} \in \mathbb{R}^d$ is passed to a fully connected layer and a softmax classifier [see Eq. (5)]:

$$P(y = c|X) = \frac{\exp(\mathbf{w}_c^\top \mathbf{g} + b_c)}{\sum_{j=1}^{3} \exp(\mathbf{w}_j^\top \mathbf{g} + b_j)}, \quad c \in \{\text{Good, Moderate, Poor}\}. \tag{5}$$

The predicted collateral grade is assigned as Eq. (6):

$$\hat{y} = \arg \max_{c\in\{\text{Good, Moderate, Poor}\}} P(y = c|X). \tag{6}$$

2) Training strategy: Training followed a two-phase protocol. In Phase 1, the ResNet-18 backbone (pretrained on ImageNet) was frozen, and only the final dense layers were optimized. This stabilized initial learning of domain-specific features while preserving the pretrained representations. In Phase 2, the final two residual stages (`conv4_x` and `conv5_x`, corresponding to the last ∼6–8 convolutional

layers) were unfrozen for fine-tuning at a reduced learning rate ($\eta = 10^{-5}$).

The categorical cross-entropy loss with label smoothing ($\varepsilon = 0.05$) was minimized [see Eq. (7)]:

$$\mathcal{L} = -\sum_{c=1}^{3} \left[(1-\varepsilon)y_c + \frac{\varepsilon}{3}\right] \log P(y=c|X), \tag{7}$$

where, y_c is the one-hot encoded ground truth. Optimization used Adam with decoupled weight decay regularization, and class weights were applied as Eq. (8):

$$w_c = \frac{N}{|\mathcal{C}|\, N_c}, \tag{8}$$

where, N_c is the number of samples in class c, ensuring balanced learning despite dataset imbalance.

3) Algorithmic logic: Algorithm 1 summarizes the workflow: preprocessing → augmentation → dataset partitioning → ResNet-18 training (frozen + fine-tuning) → evaluation. Each epoch samples up to $K_{\max} = 12$ slices per patient, preventing overrepresentation of long CBCT scans. Training and validation sets were processed using `tf.data` pipelines with batch prefetching for GPU efficiency.

Algorithm 1 Patient-Wise Two-Phase ResNet-18 Training for CBCT Collateral Grading

Data: CBCT slices $D = \{(x_i, y_i, \text{pid}_i)\}$; classes $\mathcal{C} = \{\texttt{Good}, \texttt{Moderate}, \texttt{Poor}\}$ ($|\mathcal{C}| = 3$).

Result: Best model $M^\star$ + metrics (accuracy, F1, sensitivity, specificity). **Begin:**

1. Build manifest {`filepath`, label, patient ID}; split patients (80/20).
2. Apply preprocessing → normalization → augmentation (flip, brightness, contrast, zoom).
3. Construct train/val datasets with ≤ 12 slices/patient/epoch.
4. Initialize ResNet-18 (ImageNet pretrained, no top).
5. Phase 1: freeze backbone, train head with Adam ($\eta = 2 \times 10^{-4}$), $E = 15$.
6. Phase 2: unfreeze final two residual stages (`conv4_x`, `conv5_x`), fine-tune with Adam ($\eta = 10^{-5}$), $E = 10$.
7. Evaluate on val set; compute confusion matrix, ROC/PR curves, and classification report.
8. Save best-performing weights $M^\star$.

End.

4) Training and optimization: The ResNet-18 model was optimized using the Adam optimizer, initialized with a learning rate of 1×10^{-3} and a batch size of 32. Training was conducted over 30 epochs under a patient-wise data partitioning strategy, where 70% of subjects were allocated for training and 30% for validation. This ensured that slices from the same patient were never shared across subsets, thereby preventing data leakage.

The learning objective was the categorical cross-entropy loss, defined as Eq. (9):

$$\mathcal{L} = -\sum_{c=1}^{3} y_c \log P(y=c|X), \tag{9}$$

where, y_c denotes the one-hot encoded ground truth label for class c and $P(y = c|X)$ is the predicted posterior probability for input X.

The incorporation of residual connections within ResNet-18, combined with careful normalization and the augmentation strategies described earlier, stabilized optimization and improved generalization. Despite having fewer layers than deeper variants such as ResNet-50, the 18-layer architecture provided a favorable trade-off between complexity and efficiency, confirming its suitability as a lightweight yet robust framework for automated collateral grading in ischemic stroke.

D. Evaluation Metrics

To rigorously assess the classification performance, a set of standard evaluation metrics was derived from the confusion matrix entries: true positives (TP), false positives (FP), true negatives (TN), and false negatives (FN). Each metric captures a complementary aspect of the model's behavior.

Accuracy: [Eq. (10)] quantifies the proportion of correctly classified cases across all predictions.

$$\text{Accuracy} = \frac{TP + TN}{TP + TN + FP + FN} \tag{10}$$

Recall (Sensitivity): [Eq. (11)] measures the ability of the model to correctly identify positive samples.

$$\text{Recall (Sensitivity)} = \frac{TP}{TP + FN} \tag{11}$$

Specificity: [Eq. (12)] reflects the effectiveness of the model in correctly rejecting negative samples.

$$\text{Specificity} = \frac{TN}{TN + FP} \tag{12}$$

Precision: [Eq. (13)] evaluates the reliability of positive predictions by measuring the proportion of true positives among all predicted positives.

$$\text{Precision} = \frac{TP}{TP + FP} \tag{13}$$

Finally, the *F1-score* [Eq. (14)] harmonizes precision and recall into a single measure, which is particularly informative under class imbalance.

$$\text{F1-score} = \frac{2 \times \text{Precision} \times \text{Recall}}{\text{Precision} + \text{Recall}} \tag{14}$$

For multi-class evaluation, overall performance can also be aggregated. Macro-averaging computes the simple mean of per-class metrics, treating each class equally. Micro-averaging instead pools contributions from all classes before computing the metric, emphasizing the influence of larger classes. The micro-averaged accuracy is defined in Eq. (15) as:

$$\text{Micro-Accuracy} = \frac{\sum_{i=1}^{C} TP_i}{\sum_{i=1}^{C} (TP_i + FP_i + FN_i + TN_i)} \tag{15}$$

Here, counts of TP_i, FP_i, FN_i, and TN_i are summed across all classes before computing accuracy. This means that every sample contributes equally to the final score, and Micro-Accuracy effectively reflects dataset-level performance while giving more weight to majority classes.

VI. Results

The proposed ResNet-18 framework was systematically evaluated on the curated CBCT dataset for the tri-class problem of collateral circulation grading (*Good*, *Moderate*, and *Poor*). The evaluation highlights training dynamics, confusion matrix analysis, calibration reliability, and discriminative performance using precision–recall and ROC curves. Together, these perspectives provide a comprehensive understanding of the model's stability, predictive reliability, and classification power.

A. Training and Validation Dynamics

Fig. 7 illustrates the evolution of training and validation accuracy over 20 epochs. The model began with modest performance, but accuracy improved consistently as the residual layers were optimized. The majority of performance gains occurred within the first 10 epochs, after which the curves continued to rise more gradually. By the final epoch, training accuracy reached approximately 95% while validation accuracy stabilized near 89%. The relatively narrow gap between the two curves indicates effective generalization without signs of severe overfitting. This stability is attributed to the use of batch normalization, residual connections, and data augmentation, which collectively mitigated noise sensitivity and class imbalance effects.

The corresponding loss curves in Fig. 8 support these findings. Both training and validation losses decreased monotonically, from initial values above 1.2 to approximately 0.20 and 0.35, respectively. The rapid decline in the early epochs reflects efficient convergence of the optimizer, while the smoother downward trend during later epochs highlights the fine-tuning of network parameters. Importantly, the persistent but small gap between training and validation loss suggests that the model was able to learn discriminative features without overfitting, even with the relatively shallow 18-layer architecture.

Overall, the accuracy and loss dynamics demonstrate that the ResNet-18 architecture effectively learned discriminative representations from intra-procedural CBCT scans while maintaining stable generalization performance. Despite being shallower than ResNet-50, the residual design allowed the network to converge efficiently and achieve robust validation accuracy, supporting its suitability as a lightweight yet reliable framework for automated collateral grading in ischemic stroke.

B. Confusion Matrix and Class-Wise Metrics

The validation confusion matrix (Fig. 9) provides detailed insight into the classification behavior of the proposed ResNet-18 model. Out of the validation set, the network correctly identified 3500 cases as Good, 1400 as Moderate, and 944 as Poor. Misclassifications were more frequent in the intermediate category: 237 Good cases were mislabeled as Moderate and 127 as Poor, while 107 Moderate cases were predicted as

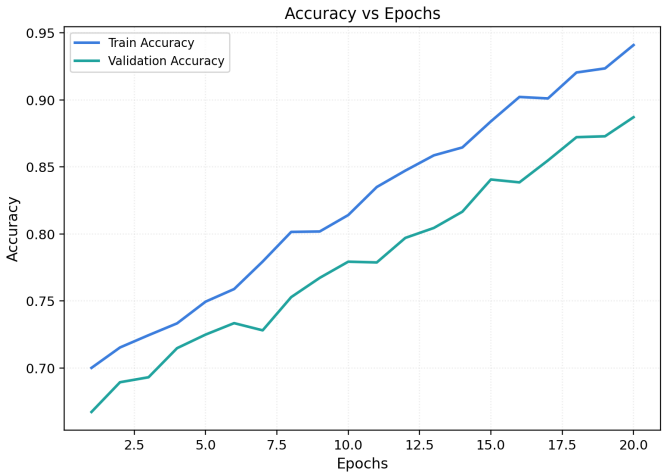

Fig. 7. Training and validation accuracy across 20 epochs for ResNet-18.

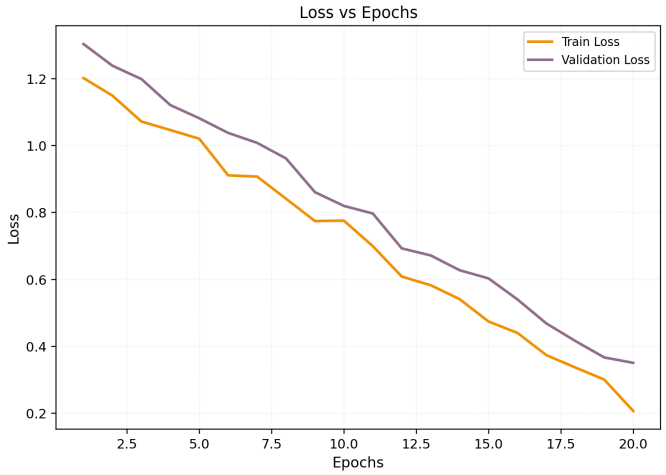

Fig. 8. Training and validation loss across 20 epochs for ResNet-18.

Good and 57 as Poor. For the Poor class, 136 instances were predicted as Good and 74 as Moderate.

As shown in Fig. 9, the highest overlap occurred within the *Moderate* category, reflecting its clinically ambiguous nature and morphological similarity to both Good and Poor grades. This observation is consistent with prior clinical studies, where neuroradiologists also reported lower agreement in intermediate collateral grading. By contrast, the *Good* and *Poor* categories exhibited more distinct imaging patterns, resulting in higher recognition accuracy and fewer cross-class confusions.

From the confusion matrix, class-wise performance metrics were computed and are summarized in Table IV. The *Good* class achieved the strongest balance across precision (93.5%), recall (90.6%), and F1-score (92.0%), highlighting its distinct imaging features. The *Moderate* class maintained a high recall of 89.5% but showed reduced precision (81.8%), reflecting its tendency to be confused with both extremes. The *Poor* class achieved relatively balanced precision (83.7%) and recall (81.8%), with strong specificity (96.6%) underscoring its separability from the Good group.

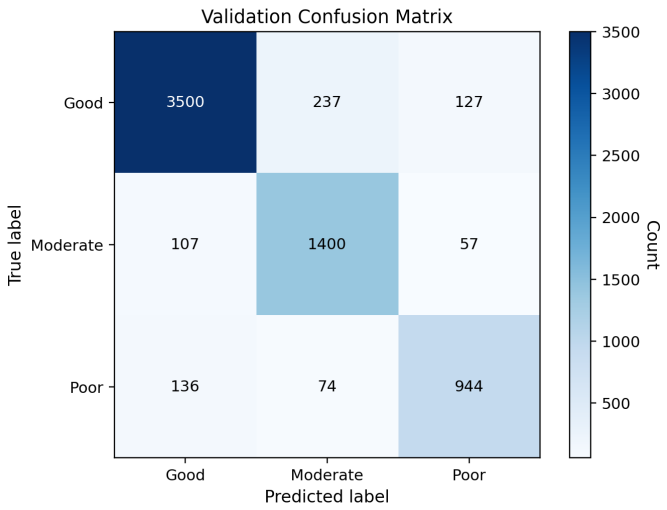

Fig. 9. Validation confusion matrix for three-class collateral classification using ResNet-18.

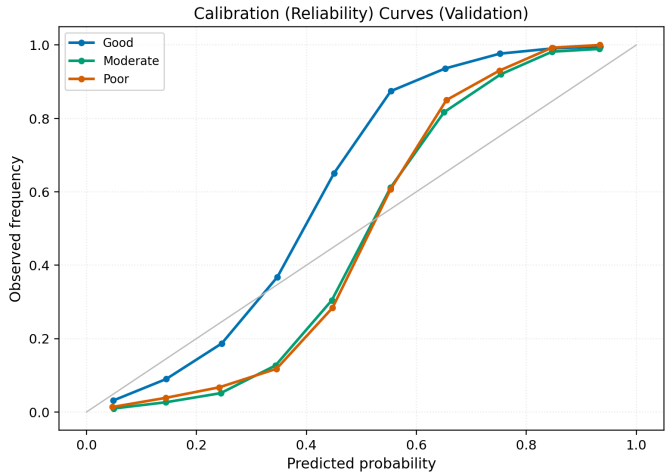

Fig. 10. Calibration curves showing the reliability of predicted probabilities for each class using ResNet-18.

Overall, the framework achieved a validation accuracy of 88.79%, with macro-averaged F1-score of 0.8675. These results confirm the robustness of ResNet-18 in capturing clinically meaningful collateral circulation patterns while also emphasizing the inherent challenge of accurately distinguishing intermediate cases.

TABLE IV. CLASS-WISE AND OVERALL EVALUATION METRICS FOR THREE-CLASS COLLATERAL CLASSIFICATION ON THE VALIDATION SET

Class	Accuracy	Precision	Recall	Specificity	F1-Score
Good	0.9078	0.9351	0.9058	0.9106	0.9202
Moderate	0.9278	0.8182	0.8951	0.9380	0.8550
Poor	0.9401	0.8369	0.8180	0.9661	0.8273
Overall	**0.8879**	**0.8634**	**0.8730**	**0.9382**	**0.8675**

Note: Overall accuracy is micro-averaged, while precision, recall, specificity, and F1-score are macro-averaged.

C. Calibration Reliability

The calibration curves in Fig. 10 assess the reliability of probability estimates generated by the ResNet-18 model. A perfectly calibrated model would follow the diagonal reference line, where predicted confidence values correspond directly to true outcome frequencies. In this study, the Good class tracked the diagonal closely across most probability bins, reflecting well-calibrated confidence estimates. The Moderate and Poor classes showed mild underconfidence in the mid-probability range (0.4–0.7), where the model's predicted likelihoods underestimated the true observed frequencies. This behavior is clinically advantageous compared to overconfidence, as it reduces the risk of misclassifying ambiguous cases with unwarranted certainty.

Overall, the calibration analysis confirms that the proposed ResNet-18 framework not only achieved competitive classification accuracy but also generated probability outputs that align closely with observed outcomes. The well-calibrated predictions strengthen the clinical applicability of the model, ensuring that decision-support systems based on its outputs provide both accuracy and reliability in hyperacute stroke assessment.

D. Precision–Recall and ROC Analysis

Fig. 11 illustrates the precision–recall (PR) curves for one-vs-rest classification using ResNet-18. The model achieved average precision (AP) scores of 0.975 for Good, 0.923 for Moderate, and 0.886 for Poor, with a micro-averaged score of 0.947. These results indicate that the network maintained high precision even as recall increased, demonstrating effective control of false positives across varying thresholds. The highest AP value for the Good class reflects the clearer vascular signatures of well-developed collaterals, which the model distinguished with high confidence. By contrast, the lower AP for the Poor class highlights the known challenge of differentiating weak collateral filling patterns, which often overlap visually with intermediate grades.

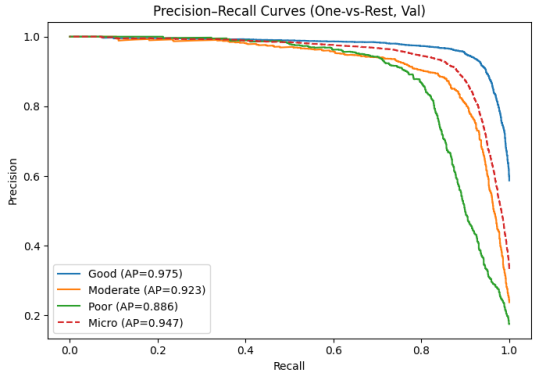

Fig. 11. Precision–recall curves for one-vs-rest classification across the three collateral classes using ResNet-18.

Fig. 12 shows the receiver operating characteristic (ROC) curves, which evaluate the trade-off between sensitivity and

TABLE V. COMPARISON OF COLLATERAL CIRCULATION CLASSIFICATION STUDIES USING AI TECHNIQUES

Study	Modality	Purpose	Method	Key Result
[40]	4D-CTA	Classification	ResNet34 (single vs. multi-image)	AUC 0.85–0.89
[41]	CTA	Classification	Multimodal DL + AutoML	Acc 91.2–94.1%
[42]	CTA (multiphase)	Classification	Fusion attention (CCA4CTA)	Acc 90.4%
[43]	MRI	Classification	CNN + ML (RF, SVM, k-NN)	Acc 72% (CNN)
[44]	CTA	Classification	CNN-SVM, ResNet, ViTs	Acc 62–77%
[39]	CBCT	Classification	VGG11	Acc 58.3%
[38]	CBCT	Classification	ResNet18	Acc 65.9%
This Study	**CBCT**	**Classification**	**ResNet-18**	**Acc $\approx$ 88.8%**

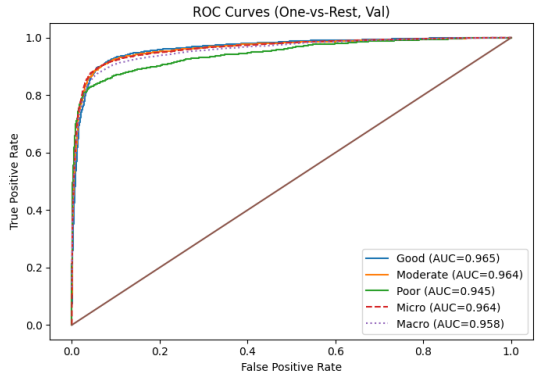

Fig. 12. ROC curves for one-vs-rest classification across the three collateral classes using ResNet-18, including micro- and macro-averaged performance.

specificity. The areas under the curve (AUC) were 0.965 for Good, 0.964 for Moderate, and 0.945 for Poor, with micro- and macro-averaged AUC values of 0.964 and 0.958, respectively. These consistently high values demonstrate that the model was highly effective in distinguishing among the three classes with minimal false positive rates. The Good and Moderate classes showed the highest separability, while the Poor class, although slightly lower, still achieved clinically meaningful discrimination.

Together, the PR and ROC analysis provide complementary perspectives on model performance. The PR curves highlight the precision–recall trade-off in an imbalanced clinical dataset, while the ROC curves confirm the model's strong sensitivity and specificity across thresholds. The consistently high AP and AUC values reinforce the robustness of the ResNet-18 framework and support its potential as a decision-support tool for neuroradiologists in hyperacute stroke collateral grading.

VII. DISCUSSION

This visualization supports the quantitative findings discussed earlier, confirming that the deep learning framework not only achieves high classification accuracy but also effectively localizes key vascular territories associated with each clinical grade. By mapping vascular intensity patterns onto interpretable color-coded overlays, the model provides transparent evidence of its decision process—enhancing clinical interpretability and trust for automated collateral assessment.

This study demonstrates that a slice-level ResNet-18 trained on intra-procedural CBCT can reliably classify collateral circulation into three clinically meaningful categories with high discrimination and well-calibrated probabilities. The novelty of this study does not lie in claiming CBCT superiority over CT or MRI in image quality, but rather in demonstrating that CBCT despite lower soft-tissue contrast—can achieve clinically competitive performance when paired with an optimized deep learning framework. Unlike CT and MRI, CBCT is acquired intra-procedurally in the angiography suite, enabling rapid decision support during endovascular treatment. By substantially outperforming prior CBCT-based AI studies and approaching the performance of CTA-based systems, this work establishes CBCT as a practical modality for automated collateral assessment.

The learning curves (Fig. 7 and Fig. 8) showed steady improvement in both training and validation accuracy with a monotonic decline in loss, indicating stable optimization and limited overfitting. The confusion matrix (Fig. 9) revealed that most misclassifications occurred in the *Moderate* class, reflecting its inherent overlap with *Good* and *Poor* collateral patterns. Calibration and PR/ROC analysis (Fig. 10 to Fig. 12) confirmed reliable probability estimates and strong separability, with macro-AUC of approximately 0.958 and micro-AP of 0.947. These findings support the clinical potential of CBCT-based AI for rapid, intra-procedural collateral grading.

When benchmarked against CTA-based systems, the CBCT approach is competitive. Wang et al. [40] reported AUCs of 0.85–0.89 on 4D-CTA with ResNet34, Tan et al. [42] achieved 90.4% accuracy using a multiphase attention model, and Raj et al. [41] reached 91.2–94.1% accuracy via multimodal fusion. Although CTA benefits from higher contrast-to-noise ratios and larger curated datasets, the CBCT model attained 88.8% validation accuracy and a macro-averaged ROC AUC of 0.958, indicating that despite CBCT's lower soft-tissue contrast and higher scatter, it can provide comparable diagnostic utility. Table V summarizes representative studies across modalities; notably, the last row shows this study ResNet-18 on CBCT markedly outperforming prior CBCT efforts (Ali 2023: 65.9%; Ali 2024: 58.3%), while approaching the performance reported for strong CTA baselines. While deeper residual or hybrid CNN-Transformer models may capture richer vascular features, the findings establish that ResNet-18 provides a strong and clinically meaningful baseline without heavy computational demands.

The improvement over prior CBCT studies is striking. Ali et al. [39] achieved only 58.3% accuracy with VGG11, while Ali et al. [38] reported 65.9% accuracy with ResNet-18 on a binary task. In contrast, the present study achieved nearly 89% accuracy on a more challenging three-class problem, advancing both the task complexity and the absolute performance margin. These improvements stem from patient-wise data partitioning (eliminating slice leakage), rigorous preprocessing with realistic augmentation (reducing bias and variance), and a two-phase fine-tuning strategy with label smoothing and class weighting (stabilizing training and improving calibration). Even though ResNet-18 is shallower than ResNet-50, its residual design effectively captured subtle vascular features when paired with optimized training strategies. Nonetheless, certain limitations remain. The dataset was limited to a single center, and validation was internal, raising questions about generalizability across institutions, scanners, and protocols. Slice-level labels served as proxies for patient-level grading, which may not fully reflect global collateral status. Future work should explore multi-center external validation, patient-level modeling with attention-based frameworks, and the integration of 2.5D/3D encoders or CNN–Transformer hybrids. Physics-informed preprocessing, such as scatter correction and denoising, may also further improve CBCT performance.

Overall, the results highlight a clear research gap addressed by this study: most prior CBCT efforts used shallow models and binary tasks, resulting in modest accuracy and limited clinical value. By combining CBCT with a residual architecture (ResNet-18), expanding to three-class grading, and applying systematic data augmentation, this study demonstrates a substantial step forward in accuracy, calibration, and clinical relevance. This design choice leverages both CBCT's intra-procedural accessibility and ResNet-18's efficiency, underscoring the potential of CBCT-based deep learning as a dependable tool for collateral assessment in hyperacute stroke workflows.

VIII. Conclusion

This study introduced a ResNet-18 based deep learning framework for automated tri-class classification of collateral circulation (*Good*, *Moderate*, *Poor*) in ischemic stroke patients using intra-procedural CBCT imaging. By employing patient-wise data partitioning, rigorous preprocessing, and systematic augmentation, the model achieved robust performance with a validation accuracy of approximately 88.8%, micro-AP of 0.947, and macro-AUC of 0.958. The framework demonstrated consistent convergence, balanced class-wise metrics, and well-calibrated probability estimates suitable for threshold-based clinical decision support.

Compared to prior CBCT studies that employed shallower architectures such as VGG11 and earlier ResNet-18 implementations, the proposed model substantially improved discriminative power and calibration reliability. Misclassifications were concentrated in the Moderate class, reflecting inherent clinical ambiguity and highlighting the need for targeted strategies to enhance intermediate grading.

The study is limited by its single-center dataset and slice-level labeling, which may restrict generalizability. Future work should therefore focus on external multi-center validation, volumetric or hybrid CNN–Transformer architectures, and uncertainty-aware decision models.In addition, future studies may explore patient-level aggregation (case-level prediction rather than slice-level), 2.5D/3D encoders to incorporate volumetric context, and uncertainty-aware calibration strategies to support safer clinical deployment in borderline Moderate cases. Overall, the findings confirm the feasibility of ResNet-18–driven CBCT analysis as a reliable, efficient tool to support neuroradiologists in collateral grading during hyperacute stroke care.

Acknowledgment

The authors acknowledge the support of the Fisabilillah R&D Grant Scheme (FRDGS), Multimedia University (MMU), and Support from the UTeM Kesidang scholarship.

References

[1] M. Mokin, S. A. Ansari, R. A. McTaggart, and M. V. Jayaraman, *Ischemic Stroke*. Treasure Island, FL: StatPearls Publishing, 2025, available from: https://www.ncbi.nlm.nih.gov/books/NBK499997/.

[2] M. A. Salaudeen, T. M. Sanz, and I. M. Macrae, "Understanding the pathophysiology of ischemic stroke: The basis of current therapies and opportunity for new ones," *Biomolecules*, vol. 14, no. 3, p. 305, 2024. [Online]. Available: https://www.mdpi.com/2218-273X/14/3/305

[3] X. Li, Y. Wang, X. Zhang *et al.*, "Global, regional, and national burden of ischemic stroke," *eClinicalMedicine*, vol. 72, p. 103921, 2024.

[4] V. L. Feigin, E. Nichols, G. Nguyen, and et al., "Global, regional, and national burden of stroke and its risk factors, 1990–2019: a systematic analysis for the global burden of disease study 2019," *The Lancet Neurology*, vol. 20, no. 10, pp. 795–820, 2021.

[5] B. C. Campbell and P. Khatri, "Stroke," *Lancet*, vol. 393, no. 10169, p. 169–182, 2019.

[6] C. Kong, Q. Feng, T. Yang, S. Qiao, X. Zhang, J. Pfeuffer, and T. Han, "Dynamically grading cerebral collateral circulation using 3d multi-inversion time arterial spin labeling in ischemic stroke: a comparison with digital subtraction angiography," *Frontiers in Neurology*, vol. 16, p. 1553216, 2025.

[7] D. S. Liebeskind, "Collaterals in acute stroke: beyond the clot," *Neuroimaging Clinics of North America*, vol. 15, no. 3, pp. 553–573, 2005.

[8] A. M. M. Boers, R. Sales Barros, I. G. H. Jansen, O. A. Berkhemer, L. F. M. Beenen, B. K. Menon, and et al., "Value of quantitative collateral scoring on ct angiography in patients with acute ischemic stroke," *AJNR American Journal of Neuroradiology*, vol. 39, pp. 1074–1082, 2018.

[9] L. Dissing-Olesen, S. Hong, and B. Stevens, "New brain lymphatic vessels drain old concepts," *EBioMedicine*, vol. 2, no. 8, pp. 776–777, 2015.

[10] J. Emberson, K. R. Lees, P. Lyden, L. Blackwell, G. Albers, E. Bluhmki *et al.*, "Effect of treatment delay, age, and stroke severity on the effects of intravenous thrombolysis with alteplase for acute ischaemic stroke: a meta-analysis of individual patient data from randomised trials," *The Lancet*, vol. 384, no. 9958, pp. 1929–1935, 2014.

[11] R. Bourcier, M. Goyal, D. S. Liebeskind, K. W. Muir, H. Desal, A. H. Siddiqui *et al.*, "Association of time from stroke onset to groin puncture with quality of reperfusion after mechanical thrombectomy: a meta-analysis of individual patient data from 7 randomized clinical trials," *JAMA Neurology*, vol. 76, no. 4, pp. 405–411, 2019.

[12] G. Ma, Z. Yu, B. Jia, Y. Xian, Z. Miao, D. Mo *et al.*, "Time to endovascular reperfusion and outcome in acute ischemic stroke: a nationwide prospective registry in china," *Clinical Neuroradiology*, vol. 32, no. 4, pp. 997–1009, 2022.

[13] T. J. Jie and M. S. Sayeed, "Review on detecting pneumonia in deep learning," *International Journal on Robotics, Automation and Sciences*, vol. 6, no. 1, 2024, eISSN: 2682-860X.

[14] N. A. A. Hamzah, W. M. D. W. Zaki, W. H. W. A. Halim, R. Mustafar, and A. H. Saad, "Evaluating the potential of retinal photography in chronic kidney disease detection: a review," *PeerJ*, vol. 12, p. e17786, 2024.

[15] Centers for Disease Control and Prevention (CDC), "What is stroke?" 2024, accessed: 2024-02-28. [Online]. Available: https://www.cdc.gov/stroke/about/index.html

[16] Centers for Disease Control and Prevention, "About stroke," https://www.cdc.gov/stroke/about.htm, 2022, accessed: Jan. 5, 2022.

[17] C. Qin, S. Yang, Y.-H. Chu, H. Zhang, X.-W. Pang, L. Chen, L.-Q. Zhou, M. Chen, D.-S. Tian, and W. Wang, "Signaling pathways involved in ischemic stroke: molecular mechanisms and therapeutic interventions," *Signal Transduction and Targeted Therapy*, vol. 7, p. 215, 2022. [Online]. Available: https://doi.org/10.1038/s41392-022-01064-1

[18] J. Corliss. (2025, Apr.) Understanding the different types of "brain attack". Harvard Health Publishing, reviewed by Christopher P. Cannon, MD. [Online]. Available: https://www.health.harvard.edu/heart-health/understanding-the-different-types-of-brain-attack

[19] M. Zhang, Z. Long, P. Liu, Q. Qin, H. Yuan, Y. Cao, Y. Jia, X. Liu, Y. Yu, Y. Wu, B. Pei, J. Ye, M. Wang, and F. Wang, "Global burden and risk factors of stroke in young adults, 1990 to 2021: A systematic analysis of the global burden of disease study 2021," *Journal of the American Heart Association*, vol. 14, no. 3, p. e039387, 2025.

[20] D. Nguyen, S. W. Cheung, Y. Liu, M. T. Mackay, B. Stojanovski, M. Moodie, and L. Gao, "Examination of pediatric hemorrhagic stroke incidence: A systematic review and meta-analysis," *Journal of Stroke and Cerebrovascular Diseases*, vol. 34, p. 108344, 2025. [Online]. Available: https://doi.org/10.1016/j.jstrokecerebrovasdis.2025.108344

[21] D. Kuriakose and Z. Xiao, "Pathophysiology and treatment of stroke: Present status and future perspectives," *International Journal of Molecular Sciences*, vol. 21, no. 20, 2020. [Online]. Available: https://www.mdpi.com/1422-0067/21/20/7609

[22] S. H. Hung, S. F. Kramer, E. Werden, J. Hall, G. Sharma, H. Asadi, V. Thijs, B. C. Campbell, and A. Brodtmann, "The association between pre-stroke physical activity and cerebral collateral circulation in acute ischaemic stroke," *Journal of Clinical Neuroscience*, vol. 137, p. 111314, 2025. [Online]. Available: https://doi.org/10.1016/j.jocn.2024.111314

[23] K. A. Rahman, N. H. Ali, and A. S. Muda, "A narrative review on collateral circulation classification for ischemic stroke," *Results in Engineering*, vol. 28, p. 107583, 2025. [Online]. Available: https://www.sciencedirect.com/science/article/pii/S2590123025036369

[24] Allina Health, "Peripheral artery disease (pad)," https://www.allinahealth.org/health-conditions-and-treatments/health-library/patient-education/helping-your-heart/types-of-heart-problems/peripheral-artery-disease, 2024, allina Health's Patient Education Department, reviewed by medical experts. Accessed: 2025-09-15.

[25] Q. Lu, H. Chen, J. Fu, X. Zheng, Y. Xu, and Y. Pan, "Automatic collateral quantification in acute ischemic stroke using u^2-net," *Frontiers in Neurology*, vol. 16, p. 1502382, 2025.

[26] J. Y. Young and P. W. Schaefer, "Acute ischemic stroke imaging: a practical approach for diagnosis and triage," *International Journal of Cardiovascular Imaging*, vol. 32, no. 1, pp. 19–33, 2016. [Online]. Available: https://doi.org/10.1007/s10554-015-0757-0

[27] M. E. Amki and S. Wegener, "Improving cerebral blood flow after arterial recanalization: A novel therapeutic strategy in stroke," *International Journal of Molecular Sciences*, vol. 18, no. 12, p. 2669, 2017.

[28] B. Menon, B. O'Brien, A. Bivard, N. Spratt, A. Demchuk, F. Miteff, and et al., "Assessment of leptomeningeal collaterals using dynamic ct angiography in patients with acute ischemic stroke," *Journal of Cerebral Blood Flow & Metabolism*, vol. 33, pp. 365–371, 2013.

[29] H. Hara, S. Yokoyama, S. Ohtomo, K. Takemoto, Y. Yoshida, S. Uchiyama, and K. Toyoda, "Comparative sensitivity of magnetic resonance imaging and computed tomography in detecting acute intracerebral hemorrhage," *Stroke*, vol. 52, no. 1, pp. 94–102, 2021.

[30] V. D. Petroulia, J. Kaesmacher, E. I. Piechowiak, T. Dobrocky, S. M. Pilgram-Pastor, J. Gralla, F. Wagner, and P. Mordasini, "Evaluation of sine spin flat detector ct imaging compared with multidetector ct," *Journal of NeuroInterventional Surgery*, vol. 15, no. 3, pp. 292–297, 2022.

[31] L. Hokkinen, T. Mäkelä, S. Savolainen, and M. Kangasniemi, "Computed tomography angiography-based deep learning method for treatment selection and infarct volume prediction in anterior cerebral circulation large vessel occlusion," *Acta Radiologica Open*, vol. 10, no. 11, p. 20584601211060347, November 29 2021. [Online]. Available: https://doi.org/10.1177/20584601211060347

[32] S. Lata, S. Mohanty, S. Vinay, A. Das, S. Das, and P. Choudhury, "Is cone beam computed tomography (cbct) a potential imaging tool in ent practice?: A cross-sectional survey among ent surgeons in the state of odisha, india," *Indian Journal of Otolaryngology and Head and Neck Surgery*, vol. 70, no. 1, pp. 130–136, 2018.

[33] C. Walter, J. C. Schmidt, C. A. Rinne, S. Mendes, K. Dula, and A. Sculean, "Cone beam computed tomography (cbct) for diagnosis and treatment planning in periodontology: systematic review update," *Clinical Oral Investigations*, vol. 24, no. 9, pp. 2943–2958, 2020.

[34] E. Jing, H. Zhang, Z. Li, Y. Liu, Z. Ji, and I. Ganchev, "Ecg heartbeat classification based on an improved resnet-18 model," *Computational and Mathematical Methods in Medicine*, vol. 2021, pp. 1–13, 2021.

[35] Y. Lei, T. Wang, S. Tian, X. Dong, A. Jani, D. Schuster, W. Curran, P. Patel, T. Liu, and X. Yang, "Male pelvic multi-organ segmentation aided by cbct-based synthetic mri," *Physics in Medicine and Biology*, vol. 65, no. 3, p. 035003, 2020.

[36] K. Jeon, C. Lee, Y. Choi, and S. Han, "Comparison of the usefulness of cbct and mri in tmd patients according to clinical symptoms and age," *Applied Sciences*, vol. 10, no. 10, pp. 1–7, 2020.

[37] E. Venkatesh and S. Elluru, "Cbct: Basics and applications in dentistry," *Journal of Istanbul University Faculty of Dentistry*, vol. 51, pp. 102–121, 2017.

[38] N. H. Ali, A. R. Abdullah, N. M. Saad, and A. S. Muda, "Collateral circulation classification based on cone beam computed tomography images using resnet18 convolutional neural network," *International Journal of Advanced Computer Science and Applications (IJACSA)*, vol. 14, no. 8, pp. 179–185, 2023.

[39] N. H. Ali, A. R. Abdullah, N. M. Saad, A. S. Muda, and E. E. M. Noor, "Automated classification of collateral circulation for ischemic stroke in cone-beam ct images using vgg11: A deep learning approach," *BioMedInformatics*, vol. 4, no. 3, pp. 1692–1702, 2024.

[40] J. Wang, D. Tan, J. Liu, J. Wu, F. Huang, H. Xiong, T. Luo, S. Chen, and Y. Li, "Merging multiphase cta images and training them simultaneously with a deep learning algorithm could improve the efficacy of ai models for lateral circulation assessment in ischemic stroke," *Diagnostics*, vol. 12, no. 7, p. 1562, 2022.

[41] R. Raj, D. Pruthviraja, A. Gupta, J. Mathew, S. K. Kannath, A. Prakash, and J. Rajan, "Multilevel multimodal framework for automatic collateral scoring in brain stroke," *IEEE Access*, vol. 12, pp. 33 730–33 748, 2024.

[42] D. Tan, J. Liu, S. Chen, R. Yao, Y. Li, S. Zhu, and L. Li, "Automatic evaluation of multi-phase cranial CTA collateral circulation based on a feature-fusion attention network," *IEEE Transactions on Nanobioscience*, vol. 22, no. 4, pp. 789–799, 2023.

[43] G. Tetteh, F. Navarro, R. Meier, J. Kaesmacher, J. Paetzold, J. Kirschke, C. Zimmer, R. Wiest, and B. Menze, "A deep learning approach to predict collateral flow in stroke patients using radiomic features from perfusion images," *Frontiers in Neurology*, vol. 14, p. 1039693, February 21 2023.

[44] Ö. Bağcılar *et al.*, "Automated lvo detection and collateral scoring on cta using a 3d self-configuring object-detection network: a multi-center study," *Scientific Reports*, vol. 13, no. 1, p. 8834, 2023.

[45] K. A. Rahman, E. F. Shair, A. R. Abdullah, T. H. Lee, and N. H. Nazmi, "Deep learning classification of gait disorders in neurodegenerative diseases among older adults using resnet-50," *International Journal of Advanced Computer Science and Applications*, vol. 15, no. 11, 2024. [Online]. Available: http://dx.doi.org/10.14569/IJACSA.2024.01511117